Surface Science 604 (2010) 1369–1376

Contents lists available at ScienceDirect

Surface Science

journal homepage: www.elsevier.com/ locate/susc

A model of oxygen adsorption at liquid copper surfaces

P. Wynblatt [a], S. Curiotto [b], D. Chatain [b,*]

[a] Department of Materials Science and Engineering, Carnegie Mellon University, Pittsburgh PA 15206, USA
[b] CNRS, Aix-Marseille University, CINAM-UPR3118, campus de Luminy, case 913, 13288 Marseille, France

ARTICLE INFO

Article history:
Received 11 March 2010
Accepted 20 April 2010
Available online 26 April 2010

Keywords:
Surface energy
Equilibrium thermodynamics
Surface segregation
Liquid copper-oxygen surfaces

ABSTRACT

A model of O-adsorption at liquid metal surfaces has been constructed, using liquid Cu as an example. The modeling approach used is similar to the regular solution scheme previously used successfully for modeling the adsorption/segregation behavior of metal alloys, in that the internal energy of the system is evaluated by nearest neighbor bond energies. In the model, the adsorption of oxygen in the near-surface region is allowed to occur at both surface and sub-surface sites. The model predicts a variety of possible adsorption characteristics, including the possibility of first order adsorption transitions which involve the formation of a 2-dimensional surface oxide, and different sequences for the occupancy of surface and sub-surface adsorption sites. In particular, by fitting the model to the experimental dependence of Cu surface energy on O-partial pressure, it is possible to conclude that O-adsorption in that case most likely occurs by the occupancy of sub-surface sites.

1. Introduction

Metals generally interact strongly with oxygen. The nature of the interaction depends on the partial pressure of oxygen (pO_2) in the atmosphere to which the metal is exposed. When the oxygen partial pressure corresponding to the limit of solubility of oxygen in the metal is exceeded, a bulk oxide becomes thermodynamically stable, whereas below that pressure, oxygen is generally adsorbed at the metal surface. In some cases, it is also possible for a two-dimensional (2-d) "surface oxide" to form within the adsorption regime, i.e. at an oxygen partial pressure lower than that corresponding to bulk oxide formation [1–4].

One important consequence of adsorption is that it decreases surface energy, thereby affecting all capillarity-related behavior [5,6]. Other types of behavior may also be modified. For example, it has recently been suggested that the formation of 2-d surface oxides may improve the catalytic performance of copper when it is used to catalyze the oxidation of gas phase species [4].

There has been considerable interest in modeling adsorption/segregation phenomena at metal surfaces. Previous work has generally used one of three approaches: computer simulations which make use of semi-empirical interaction potentials [7,8], first principles calculations [9], and analytical thermodynamic models [10–13]. The first two approaches have tended to address adsorption energies, and the manner in which surface structure changes with adsorption. On the other hand, the thermodynamic approach has been based on a simplified description of the surface structure and has focused on estimates of the dependence of adsorption on the chemical potential of the adsorbing species, and on the resulting changes in surface energy.

In this paper, we make use of the thermodynamic approach to investigate oxygen adsorption at the surface of liquid copper. In metal alloy systems, this type of modeling uses the heat of mixing to quantify the interaction between the alloy components, and the surface energy of the pure components to quantify the surface energy of the (segregated) alloy [12,14,15]. In the present case of adsorption from the gas phase, several technical difficulties need to be resolved. (i) The sites occupied by oxygen in copper need to be defined; (ii) the best method to formulate realistic copper–oxygen interactions is not obvious; and (iii) a means must be found to define the contribution to the surface energy of an adsorbed "oxygen entity".

A great deal of work has been performed on the location of adsorbed oxygen on copper surfaces of different orientations, using ultra-high vacuum (UHV) experimental approaches such as low energy electron diffraction, scanning tunneling microcopy, Auger electron spectroscopy, etc. As will be described in more detail below, the density and degree of close packing of a liquid surface is quite similar to that of the (111) surface of a face centered cubic (FCC) metal [16–19]. Thus, some indications on the behavior of adsorbed oxygen on a liquid copper surface could in principle be obtained from studies of oxygen adsorption on Cu(111). However, in UHV work, oxygen is adsorbed on the surface by exposing samples to a known flux of oxygen, until the desired oxygen coverage is obtained. Thus, no relation is obtained between oxygen adsorption and oxygen chemical potential.

In contrast to the surface science methodology, measurements aimed at the determination of surface energy of liquid copper have

* Corresponding author. Tel.: +33 660302890; fax: +33 491418916.
E-mail addresses: pw01@andrew.cmu.edu (P. Wynblatt), curiotto@cinam.univ-mrs.fr (S. Curiotto), chatain@cinam.univ-mrs.fr (D. Chatain).

0039-6028/$ – see front matter © 2010 Elsevier B.V. All rights reserved.
doi:10.1016/j.susc.2010.04.015

been performed under a well-defined oxygen chemical potential. In these experiments the liquid copper surface is exposed to a mixture of gases that produce a given pO_2 [20–23], and the surface energy is measured by the sessile drop technique. However, these measurements suffer from the disadvantage that O-adsorption is not measured directly.

Several previous attempts have been made at modeling O-adsorption at liquid metal surfaces by the thermodynamic approach, [6,24,25]. These studies have made use of the Gibbs adsorption isotherm, which may be expressed as follows:

$$\gamma_M = \gamma_M^0 - \Gamma_M \mu_M - \Gamma_O \mu_O$$

where γ_M is the surface energy, γ_M^0 is the surface energy of the pure metal M, Γ_j is the adsorption of the species j (O and M), and μ_j, the chemical potential of the jth species. Ricci et al. [24] and Eustathopoulos et al. [25] have used a concept developed by Wagner [26] in which oxygen is described as an oxide cluster dissolved in a sea of metal. This so-called "coordination cluster theory" provides a good description of the bulk thermodynamics of oxygen dissolved in metals and alloys [27–29]. Saiz et al. [6] have followed the approach of Belton [30], in which the Langmuir adsorption isotherm is combined with the Gibbs adsorption isotherm. That approach uses experimental data on the relationship between surface energy and oxygen potential to evaluate adsorption, and cannot therefore be used to predict adsorption behavior independently of adsorption-related experimental information.

The model presented in this paper aims to link the macroscopic approach of previous authors [6,24,25] to a mean-field atomic description of the surface thermodynamics of oxygen at the surface of liquid copper. It is similar to the Belton approach in that we combine Gibbsian adsorption with a Langmuir-like model. However, unlike the classical Langmuir approach, our model does not limit adsorption to a single type of adsorption site, and we have avoided the assumption that the adsorption coefficient is independent of coverage. In addition, while the data used as input to the model is derived from experimental measurements of surface energies of the relevant pure components, none of the input data is either directly or indirectly related to O-adsorption.

2. Model

2.1. General structure

The approach used here is similar to the regular solution scheme previously used successfully for modeling the adsorption (or interfacial segregation) behavior of metal alloys [10–12,14]. In that approach, the energy due to interactions between the two species (Cu and O) is approximated by nearest neighbor bond energies and the entropy is taken to be that of an ideal solution. Such a method is reasonable for the description of systems such as Cu–O, where the interactions are predominantly covalent, but would not be appropriate, for example, in Mg–O, where the interactions are predominantly ionic, especially if there is a possibility for the formation of 2-d oxides at the surface.

We will consider O-adsorption to the surface of a Cu liquid. For convenience, we will assume that the atoms of the liquid occupy a FCC lattice. This type of approximation for liquids has often been adopted in the past [11,13] and has yielded favorable comparisons with experimental results of adsorption at liquid surfaces. In addition, such an assumption is not unreasonable, because the coordination in liquid metals that are close-packed in the solid state is ~11 [31], and therefore not very different from that in their crystalline form. Furthermore, the arrangement of Cu-atoms at the pure liquid surface will be taken to correspond to the structure of a FCC (111) surface, as it has been shown both experimentally [18,19] and by computer modeling [16,17] that liquid metal surfaces are more ordered than the bulk liquid over regions a few atom diameters in thickness, and that these ordered regions are also more densely packed than the adjacent bulk liquid. In general, this surface ordering is expected to prevail only in the vicinity of the melting point. However, measurements of liquid surface ordering in Ga [19] have shown that detectable ordering can persist to temperatures of up to 150 K above the melting temperature. In the present study we will confine application of the model to a temperature of 1365 K, where most of the relevant surface energy measurements have been made. This temperature is only 7 K above the melting point of Cu.

As the oxygen potential in equilibrium with bulk liquid Cu is increased, the concentration of oxygen dissolved in Cu also increases. When the oxygen potential reaches the value corresponding to the oxygen solubility limit, the Cu_2O phase forms. Depending on temperature, Cu_2O can be either liquid or solid. We shall focus here on the temperature domain where bulk Cu_2O is solid. In solid Cu_2O, Cu-atoms occupy the sites of a FCC lattice, and the O-atoms occupy 2 of the 8 tetrahedral holes of the Cu structure, as shown schematically in Fig. 1 (space group: Pn3m, lattice constant: 0.4267 nm [32]). The O-sites in Cu_2O have also been found to be the preferred O-adsorption sites at the Cu(111) surface by first principles calculations [4]. For the purposes of the current model, we assume that O-atoms dissolved in Cu also occupy the same type of O-sites as in Cu_2O.

We use the structure of the $Cu_2O(111)$ surface as a guide for the structure of the Cu surface containing adsorbed O. The $Cu_2O(111)$ surface can be viewed as consisting of a FCC stacking of (111) Cu-planes with O-sites lying both above and below these planes. The two types of O-sites will be referred to as upper and lower sites, as illustrated schematically in Figs. 1 and 2. It is also useful to number the Cu layers with a superscript i, $Cu^{(i)}$, where $i=1$ refers to the surface Cu layer. The upper O-sites associated with $Cu^{(1)}$ will be labeled O1. These lack one of their four Cu-neighbors and four of their eight nearest O-neighbors. The lower O-sites associated with $Cu^{(1)}$ are labeled O2. These have their full complement of Cu-neighbors but only seven of their eight O-neighbors. We consider that segregation of oxygen at the Cu surface occurs by populating O1 and O2 sites adjacent to $Cu^{(1)}$. O-sites associated with planes $Cu^{(i)}$, having $i>1$, are taken to have the bulk O-site fraction. Since O-atoms dissolved in Cu as well as O-atoms in Cu_2O are assumed to occupy their own sublattice, O-segregation occurs by populating the near-surface O-sublattice and does not require any redistribution of Cu-atoms on the Cu-sublattice.

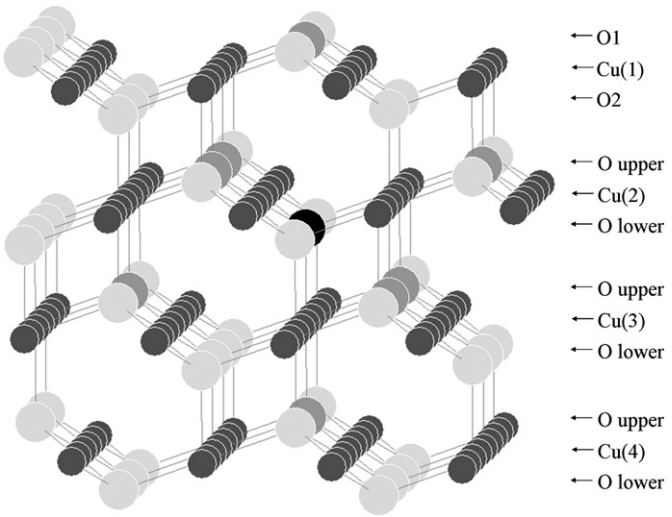

Fig. 1. Crystal structure of Cu_2O. Small and large circles represent the Cu and O-atoms, respectively. The first four near-surface copper planes, $Cu^{(i)}$ ($i=1$ to 4), of a (111)-oriented surface are shown together with their associated O-atoms. Only O–Cu bonds are indicated. The black O-atom (blue on line) is used to illustrate the O–O coordination, by shading its O-neighbors in dark grey (medium blue on line).

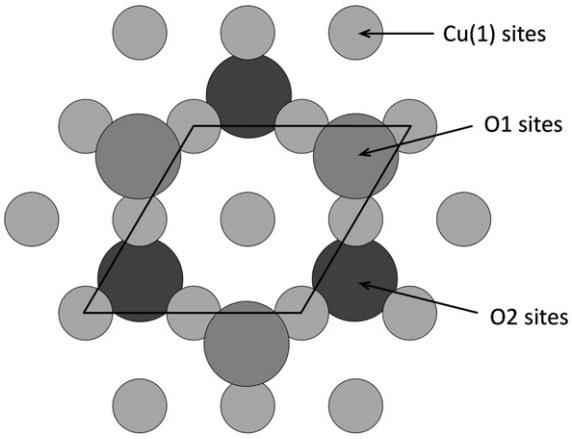

Fig. 2. Cu_2O structure viewed along [111] axis. Small and large circles represent the Cu and O-atoms, respectively. The surface unit cell is indicated by the lozenge.

The internal energy of the segregated system is calculated by means of a nearest neighbor bond model. We consider the following types of bonds. The Cu-neighbors of an O-atom are considered "special" in the sense that there may be some electronic interaction between them and the adjacent O-atom. Thus, these Cu-atoms are labeled Cu′, and the energy of Cu′–O bonds is labeled $\varepsilon_{Cu'O}$. Similarly, the energy of bonds connecting two special Cu′-atoms are labeled $\varepsilon_{Cu'Cu'}$, and those between a Cu′-atom and an "ordinary" Cu-atom are labeled $\varepsilon_{Cu'Cu}$. Finally, the bonds between nearest neighbor O-atoms are labeled ε_{OO}, and those between a pair of ordinary Cu-atoms are labeled ε_{CuCu}. Note that a Cu-atom in the segregated layer can have up to two O-neighbors. However, Cu-atoms have been labeled Cu′, whether they have one or two O-neighbors. This simplification has been made in order to avoid proliferation of bond energy types (such as $\varepsilon_{Cu''Cu}$, $\varepsilon_{Cu''Cu'}$, etc.) because, as will be seen later, there is only limited data available to define the bond energies.

Entropy contributions associated with the distribution of O-atoms on O-sites, is computed in the ideal solution approximation, and the internal energy due to bonds is computed assuming a random distribution of O-atoms on O-sublattice sites.

The equilibrium surface composition is obtained by minimizing the surface energy w.r.t. the fractions of occupied O1 and O2 sites. The advantage of this approach is that it naturally yields the surface energy of the system as a function of O-adsorption.

2.2. Equilibrium surface composition

The number of O-sites in each set of upper and lower O-sites associated with a given Cu plane is defined as N_O in units of moles per unit surface area. The number of Cu-sites/area in each Cu plane is defined as N_{Cu} in the same units. Thus, from the structure of Fig. 1, we have:

$$4N_O = N_{Cu} \tag{1}$$

The fractions of occupied O1 and O2 sites (associated with $Cu^{(1)}$) are X_{O1} and X_{O2}, respectively, and the fraction of occupied O-sites associated with all other Cu-planes is X_{Ob}, corresponding to the fractional occupancy of O in a bulk layer. As noted above, Cu species may be identified as Cu or Cu′. It is convenient to define the fractions of Cu–Cu, Cu′–Cu and Cu′–Cu′ bonds in each Cu layer as $f^{(i)}{}_{CuCu}$, $f^{(i)}{}_{Cu'Cu}$ and $f^{(i)}{}_{Cu'Cu'}$, respectively, where the superscript i indicates the plane $Cu^{(i)}$. O-atoms occupying O2 sites of the $Cu^{(1)}$ plane have Cu-neighbors in the $Cu^{(2)}$ plane, and thus modify the fractions of Cu and Cu′ atoms in that plane. As a result, the interactions between Cu-atoms occupying the $Cu^{(1)}$ and $Cu^{(2)}$ planes, as well as the $Cu^{(2)}$ and $Cu^{(3)}$ planes, are also modified. To address this issue, we also define the fractions of the three types of bonds that connect Cu-atoms in adjacent $Cu^{(i)}$ and $Cu^{(j)}$ planes as $f^{(i-j)}{}_{hk}$ (h,k = Cu,Cu′). Finally, it should be mentioned that O-atoms have first neighbor O-sites which lie as far as three O-layers away, as shown in Fig. 1. Thus, for example, O-atoms in the O2 layer have O-neighbors which lie in the upper O-sites of both $Cu^{(2)}$ and $Cu^{(3)}$ planes.

We express the surface energy as the surface excess grand potential:

$$\gamma = e^S - Ts^S - \sum_j \Gamma_j \mu_j \tag{2}$$

where γ is the surface energy, e^S and s^S are the surface excess internal energy and entropy per unit area, respectively, and Γ_j and μ_j are the adsorption and chemical potential of the jth component (j = Cu, O). Since there is no surface excess of Cu in the present problem, i.e. the number of Cu-atoms per unit area remains the same in the near-surface layers as in the bulk layers, Γ_{Cu} vanishes, and the sum of Eq. (2) reduces to $\Gamma_O\mu_O$.

Let us now consider a system consisting of 3 Cu surface planes ($Cu^{(i)}$, $i = 1, 2, 3$) attached to M bulk-like Cu layers. We write the surface excess terms of Eq. (2) by subtracting the free energy of (M + 3) bulk layers from that of the system under consideration. This leads to identical cancellation of the free energies of the M bulk layers, leaving the energy of the three surface layers, less the free energy of three bulk layers. Thus, γ may be expressed as:

$$\begin{aligned}
\gamma = {} & N_O[3X_{O1}\varepsilon_{Cu'O} + 4X_{O2}\varepsilon_{Cu'O} + 3X_{O1}X_{O2}\varepsilon_{OO} + 0.5X_{O1}X_{Ob}\varepsilon_{OO} \\
& + 2X_{O2}X_{Ob}\varepsilon_{OO}] \\
& + 3N_{Cu}\left[f^{(1)}{}_{CuCu}\varepsilon_{CuCu} + f^{(1)}{}_{Cu'Cu}\varepsilon_{Cu'Cu} + f^{(1)}{}_{Cu'Cu'}\varepsilon_{Cu'Cu'}\right] \\
& + 3N_{Cu}\left[f^{(1-2)}{}_{CuCu}\varepsilon_{CuCu} + f^{(1-2)}{}_{Cu'Cu}\varepsilon_{Cu'Cu} + f^{(1-2)}{}_{Cu'Cu'}\varepsilon_{Cu'Cu'}\right] \\
& + N_O RT[X_{O1}\ln(X_{O1}) + (1-X_{O1})\ln(1-X_{O1}) + X_{O2}\ln(X_{O2}) \\
& + (1-X_{O2})\ln(1-X_{O2})] \\
& + N_O\left[8X_{Ob}\varepsilon_{Cu'O} + 1.5X_{Ob}X_{O2}\varepsilon_{OO} + 0.5X_{Ob}X_{O1}\varepsilon_{OO} + 5.5X_{Ob}^2\varepsilon_{OO}\right] \\
& + 3N_{Cu}\left[f^{(2)}{}_{CuCu}\varepsilon_{CuCu} + f^{(2)}{}_{Cu'Cu}\varepsilon_{Cu'Cu} + f^{(2)}{}_{Cu'Cu'}\varepsilon_{Cu'Cu'}\right] \\
& + 3N_{Cu}\left[f^{(2-3)}{}_{CuCu}\varepsilon_{CuCu} + f^{(2-3)}{}_{Cu'Cu}\varepsilon_{Cu'Cu} + f^{(2-3)}{}_{Cu'Cu'}\varepsilon_{Cu'Cu'}\right] \\
& + 2N_O RT[X_{Ob}\ln(X_{Ob}) + (1-X_{Ob})\ln(1-X_{Ob})] \\
& + N_O\left[8X_{Ob}\varepsilon_{Cu'O} + 0.5X_{Ob}X_{O2}\varepsilon_{OO} + 7.5X_{Ob}^2\varepsilon_{OO}\right] \\
& + 3N_{Cu}\left[f^{(b)}{}_{CuCu}\varepsilon_{CuCu} + f^{(b)}{}_{Cu'Cu}\varepsilon_{Cu'Cu} + f^{(b)}{}_{Cu'Cu'}\varepsilon_{Cu'Cu'}\right] \\
& + 1.5N_{Cu}\left[f^{(b)}{}_{CuCu}\varepsilon_{CuCu} + f^{(b)}{}_{Cu'Cu}\varepsilon_{Cu'Cu} + f^{(b)}{}_{Cu'Cu'}\varepsilon_{Cu'Cu'}\right] \\
& + 2N_O RT[X_{Ob}\ln(X_{Ob}) + (1-X_{Ob})\ln(1-X_{Ob})] \\
& - 3\{2N_O X_{Ob}[4X_{Ob}\varepsilon_{OO} + 4\varepsilon_{Cu'O}] \\
& + 6N_{Cu}\left[f^{(b)}{}_{CuCu}\varepsilon_{CuCu} + f^{(b)}{}_{Cu'Cu}\varepsilon_{Cu'Cu} + f^{(b)}{}_{Cu'Cu'}\varepsilon_{Cu'Cu'}\right] \\
& + 2N_O RT[X_{Ob}\ln(X_{Ob}) + (1-X_{Ob})\ln(1-X_{Ob})]\} \\
& - \Gamma_O\mu_O
\end{aligned} \tag{3}$$

Here, $f^{(b)}{}_{hk}$ is the fraction of bonds of the various types in a bulk-like layer. Note that there is no difference between in-layer bond fractions $f^{(b)}{}_{hk}$ and interlayer bond fractions $f^{(b-b)}{}_{hk}$. The first term in Eq. (3) accounts for the bond energies of the interactions between O-atoms in O1 and O2 sites with other O-atoms and with Cu-atoms (as an example, an explanation of how these values are obtained is given in Appendix I), the second term represents the bond energies within plane $Cu^{(1)}$, and the third term gives the energies of the bonds between the $Cu^{(1)}$ and $Cu^{(2)}$ planes. The fourth term gives the entropy of mixing of the O1 and O2 atoms on the O-sublattice. There is no

entropy associated with mixing of Cu and Cu′ on Cu-sublattice sites, because that distribution is determined by the distribution of the adjacent O-atoms, and is not independent. The next four terms represent the equivalent quantities for the $Cu^{(2)}$ plane. The following four terms give the same quantities for the $Cu^{(3)}$ plane, except that only half of its interaction with layer $Cu^{(4)}$ is included, as the other half was subtracted with the free energy of the M bulk layers to obtain the surface excess free energy. The next three terms of Eq. (3) represent the free energy of the 3 bulk layers that are subtracted to yield the surface excess free energy. The last term subtracts the adsorption and chemical potential term.

The various terms $f^{(i)}{}_{hk}$ and $f^{(i-j)}{}_{hk}$, are not always easy to calculate, because of the awkward geometry of the Cu_2O structure. In many cases they had to be evaluated by averaging over many simulations in which O-atoms were distributed at random among the various sites. The standard deviations of the values obtained by the simulations were typically about 10% of the mean values. However, the mean values are robust, and are the only significant values needed in such a mean-field model. The values obtained are summarized in Table 1, where all the bond fractions are expressed as functions of the principal composition variables: X_{O1}, X_{O2} and X_{Ob}.

One minor inconsistency in Eq. (3) should be noted. O-atoms occupying upper O-sites of the $Cu^{(2)}$ layer have one dangling O–O bond (due to the presence of the surface), and the O-concentration of that layer should therefore strictly be considered to be variable. This has been ignored in the present model, and the fraction of occupied O-sites in that layer has been set to X_{Ob}.

We now turn to an evaluation of the last terms in Eq. (3), namely: the O-adsorption, and the O-chemical potential. The O-adsorption is just the surface excess number of moles of O per unit area, and may be written:

$$\Gamma_O = N_O(X_{O1} + X_{O2} - 2X_{Ob}) \tag{4}$$

The chemical potential is somewhat more involved, and requires the definition of some additional terms. Thus far, we have described the bulk composition in terms of X_{Ob}, the fraction of occupied O-sites in the O-sublattice associated with planes $Cu^{(i)}$ ($i>1$). It is convenient to redefine the bulk composition of the Cu–O alloy in terms of the conventional atom fraction of oxygen, which we shall denote as X_O^C (the superscript C standing for "conventional"). The relationships between X_{Ob} and X_O^C are:

$$X_O^C = \frac{X_{Ob}}{2 + X_{Ob}}, \text{ or } X_{Ob} = \frac{2X_O^C}{1 - X_O^C} \tag{5}$$

We also need to write an expression for the bulk free energy of the Cu–O alloy. This can be extracted from Eq. (3) where we included terms for the free energy of three bulk Cu layers with their associated O-atoms. The free energy of a single bulk layer is defined as $F^b(X_{Ob})$:

$$\begin{aligned} F^b(X_{Ob}) = {} & 2N_O X_{Ob}[4X_{Ob}\varepsilon_{OO} + 4\varepsilon_{Cu'O}] \\ & + 24N_O\left[f^{(b)}{}_{CuCu}\varepsilon_{CuCu} + f^{(b)}{}_{Cu'Cu}\varepsilon_{Cu'Cu} + f^{(b)}{}_{Cu'Cu'}\varepsilon_{Cu'Cu'}\right] \\ & + 2N_O RT[X_{Ob}\ln(X_{Ob}) + (1-X_{Ob})\ln(1-X_{Ob})] \end{aligned} \tag{6}$$

where Eq. (1) has been used to eliminate N_{Cu}. For an alloy of bulk composition X_O^C, the free energy of 1 mol of bulk solution, F_m, is given by X_O^C times the bulk free energy per mole of O (i.e. $F^b(X_{Ob})$ divided by $2N_OX_{Ob}$):

$$F_m = X_O^C\frac{F^b(X_{Ob})}{2N_OX_{Ob}} = \frac{F^b(X_{Ob})}{2N_O(2 + X_{Ob})} \tag{7}$$

This expression is used in Appendix II to demonstrate that the O-chemical potential can be expressed as:

$$\begin{aligned} \mu_O = {} & [8X_{Ob}\varepsilon_{OO} + 4\varepsilon_{Cu'O}] + 12\left[\frac{\partial f^{(b)}_{CuCu}}{\partial X_{Ob}}\varepsilon_{CuCu} + \frac{\partial f^{(b)}_{Cu'Cu}}{\partial X_{Ob}}\varepsilon_{Cu'Cu} + \frac{\partial f^{(b)}_{Cu'Cu'}}{\partial X_{Ob}}\varepsilon_{Cu'Cu'}\right] \\ & + RT[\ln(X_{Ob}/(1-X_{Ob}))] \end{aligned} \tag{8}$$

The equilibrium values of X_{O1} and X_{O2}, corresponding to O-adsorption at the Cu surface, are obtained by minimizing Eq. (3), together with the definitions of Γ_O and μ_O of Eqs. (4) and (8). This yields:

$$\begin{aligned} & RT[\ln(X_{O1}/(1-X_{O1}))] + [3X_{O2}\varepsilon_{OO} + 3\varepsilon_{Cu'O} + X_{Ob}\varepsilon_{OO}] \\ & + 12\left[\frac{\partial f^{(1)}_{CuCu}}{\partial X_{O1}}\varepsilon_{CuCu} + \frac{\partial f^{(1)}_{Cu'Cu}}{\partial X_{O1}}\varepsilon_{Cu'Cu} + \frac{\partial f^{(1)}_{Cu'Cu'}}{\partial X_{O1}}\varepsilon_{Cu'Cu'}\right] \\ & + 12\left[\frac{\partial f^{(1)(2)}_{CuCu}}{\partial X_{O1}}\varepsilon_{CuCu} + \frac{\partial f^{(1)(2)}_{Cu'Cu}}{\partial X_{O1}}\varepsilon_{Cu'Cu} + \frac{\partial f^{(1)(2)}_{Cu'Cu'}}{\partial X_{O1}}\varepsilon_{Cu'Cu'}\right] \\ & + 12\left[\frac{\partial f^{(2)}_{CuCu}}{\partial X_{O1}}\varepsilon_{CuCu} + \frac{\partial f^{(2)}_{Cu'Cu}}{\partial X_{O1}}\varepsilon_{Cu'Cu} + \frac{\partial f^{(2)}_{Cu'Cu'}}{\partial X_{O1}}\varepsilon_{Cu'Cu'}\right] \\ & - RT[\ln(X_{Ob}/(1-X_{Ob}))] - [8X_{Ob}\varepsilon_{OO} + 4\varepsilon_{Cu'O}] \\ & - 12\left[\frac{\partial f^{(b)}_{CuCu}}{\partial X_{Ob}}\varepsilon_{CuCu} + \frac{\partial f^{(b)}_{Cu'Cu}}{\partial X_{Ob}}\varepsilon_{Cu'Cu} + \frac{\partial f^{(b)}_{Cu'Cu'}}{\partial X_{Ob}}\varepsilon_{Cu'Cu'}\right] = 0 \end{aligned} \tag{9a}$$

Table 1
Bond fractions for near-surface Cu-planes, and for bulk Cu-planes, in terms of the fractions of occupied O-sites.

Bond fractions	Values
$f^{(1)}{}_{CuCu}$	$1-0.5X_{Ob}-1.25X_{O1}-1.25X_{O2}+0.25X_{O1}{}^2+0.25X_{O2}{}^2+0.5X_{Ob}X_{O1}+0.5X_{Ob}X_{O2}+1.5X_{O1}X_{O2}-0.25X_{O2}X_{O1}{}^2-0.25X_{O1}X_{O2}{}^2-0.5X_{Ob}X_{O1}X_{O2}$
$f^{(1)}{}_{Cu'Cu}$	$0.5X_{Ob}+X_{O1}+X_{O2}-0.5X_{O1}{}^2-0.5X_{O2}{}^2-X_{Ob}X_{O1}-X_{Ob}X_{O2}-1.5X_{O1}X_{O2}+0.5X_{O1}X_{O2}{}^2+0.5X_{O2}X_{O1}{}^2+X_{Ob}X_{O1}X_{O2}$
$f^{(1)}{}_{Cu'Cu'}$	$0.25X_{O1}+0.25X_{O2}+0.25X_{O1}{}^2+0.25X_{O2}{}^2+0.5X_{Ob}X_{O1}+0.5X_{Ob}X_{O2}-0.25X_{O1}X_{O2}{}^2-0.25X_{O2}X_{O1}{}^2-0.5X_{Ob}X_{O1}X_{O2}$
$f^{(1-2)}{}_{CuCu}$	$1-1.75X_{Ob}-0.75X_{O1}-0.75X_{O2}+1.25X_{Ob}X_{O1}+1.25X_{Ob}X_{O2}+0.75X_{O1}X_{O2}-1.25X_{Ob}X_{O1}X_{O2}$
$f^{(1-2)}{}_{Cu'Cu}$	$1.5X_{Ob}+0.75X_{O1}-2.5X_{Ob}X_{O1}+0.5X_{O2}-2.25X_{Ob}X_{O2}-0.75X_{O1}X_{O2}+2.5X_{Ob}X_{O1}X_{O2}$
$f^{(1-2)}{}_{Cu'Cu'}$	$0.25X_{Ob}+0.25X_{O2}+X_{Ob}X_{O2}+1.25X_{Ob}X_{O1}-1.25X_{Ob}X_{O1}X_{O2}$
$f^{(2)}{}_{CuCu}$	$1-2.75X_{Ob}-0.5X_{O2}+1.25X_{Ob}X_{O2}$
$f^{(2)}{}_{Cu'Cu}$	$2.25X_{Ob}+0.5X_{O2}-0.5X_{Ob}{}^2-2.25X_{Ob}X_{O2}$
$f^{(2)}{}_{Cu'Cu'}$	$0.5X_{Ob}+X_{Ob}X_{O2}+0.5X_{Ob}{}^2$
$f^{(2-3)}{}_{CuCu}$	$1-3.25X_{Ob}-0.25X_{O2}+3.75X_{Ob}{}^2+0.5X_{Ob}X_{O2}$
$f^{(2-3)}{}_{Cu'Cu}$	$2.75X_{Ob}+0.25X_{O2}-5.75X_{Ob}{}^2-0.75X_{Ob}X_{O2}$
$f^{(2-3)}{}_{Cu'Cu'}$	$0.5X_{Ob}+2X_{Ob}{}^2+0.25X_{Ob}X_{O2}$
$f^{(b)}{}_{CuCu}$	$1-3.5X_{Ob}+4.5X_{Ob}{}^2-2.5X_{Ob}{}^3+0.5X_{Ob}{}^4$
$f^{(b)}{}_{Cu'Cu}$	$3X_{Ob}-7X_{Ob}{}^2+5X_{Ob}{}^3-X_{Ob}{}^4$
$f^{(b)}{}_{Cu'Cu'}$	$0.5X_{Ob}+2.5X_{Ob}{}^2-2.5X_{Ob}{}^3+0.5X_{Ob}{}^4$

and

$$RT[\ln(X_{O2}/(1-X_{O2}))] + [3X_{O1}\varepsilon_{OO} + 4\varepsilon_{Cu'O} + 4X_{Ob}\varepsilon_{OO}] + 12\left[\frac{\partial f^{(1)}_{CuCu}}{\partial X_{O2}}\varepsilon_{CuCu} + \frac{\partial f^{(1)}_{Cu'Cu}}{\partial X_{O2}}\varepsilon_{Cu'Cu} + \frac{\partial f^{(1)}_{Cu'Cu'}}{\partial X_{O2}}\varepsilon_{Cu'Cu'}\right] + 12\left[\frac{\partial f^{(1)(2)}_{CuCu}}{\partial X_{O2}}\varepsilon_{CuCu} + \frac{\partial f^{(1)(2)}_{Cu'Cu}}{\partial X_{O2}}\varepsilon_{Cu'Cu} + \frac{\partial f^{(1)(2)}_{Cu'Cu'}}{\partial X_{O2}}\varepsilon_{Cu'Cu'}\right] + 12\left[\frac{\partial f^{(2)}_{CuCu}}{\partial X_{O2}}\varepsilon_{CuCu} + \frac{\partial f^{(2)}_{Cu'Cu}}{\partial X_{O2}}\varepsilon_{Cu'Cu} + \frac{\partial f^{(2)}_{Cu'Cu'}}{\partial X_{O2}}\varepsilon_{Cu'Cu'}\right] + 12\left[\frac{\partial f^{(2)(3)}_{CuCu}}{\partial X_{O2}}\varepsilon_{CuCu} + \frac{\partial f^{(2)(3)}_{Cu'Cu}}{\partial X_{O2}}\varepsilon_{Cu'Cu} + \frac{\partial f^{(2)(3)}_{Cu'Cu'}}{\partial X_{O2}}\varepsilon_{Cu'Cu'}\right] - RT[\ln(X_{Ob}/(1-X_{Ob}))] - [8X_{Ob}\varepsilon_{OO} + 4\varepsilon_{Cu'O}] - 12\left[\frac{\partial f^{(b)}_{CuCu}}{\partial X_{Ob}}\varepsilon_{CuCu} + \frac{\partial f^{(b)}_{Cu'Cu}}{\partial X_{Ob}}\varepsilon_{Cu'Cu} + \frac{\partial f^{(b)}_{Cu'Cu'}}{\partial X_{Ob}}\varepsilon_{Cu'Cu'}\right] = 0 \quad (9b)$$

The equilibrium surface compositions are obtained by solving Eqs. (9a) and (9b) simultaneously for X_{O1} and X_{O2}.

2.3. Evaluation of bond energies

We evaluate the bond energies from the surface energies of Cu and Cu_2O. Although bond energies could in principle also be evaluated from chemical reactions, such as:

$$1/2O_2(g) + 2Cu(l) = Cu_2O(s),$$

it is preferable to perform the assessment of bond energies from surface energies, when the purpose is to evaluate surface properties.

We obtain the Cu–Cu bond energy from the surface energy of liquid Cu, under the assumption that the liquid surface has the same structure as the (111) surface of the solid. Close to its melting point, the surface energy of liquid Cu is 1.37 J/m^2 which is an average of the experimental values reported later in Fig. 5. Taking into account that 3 bonds per atom are broken to create 2 Cu surfaces, that the lattice constant of Cu is $a_{Cu}=0.3615$ nm [32], and that the area occupied by a Cu atom at the (111) surface is $(a_{Cu})^2\sqrt{3}/4$, one obtains

$$\varepsilon_{CuCu} = 1.37\left[J/m^2\right](a_{Cu})^2/(2\sqrt{3})\left[m^2/atom\right]\left(6.02\times10^{23}[atom/mol]\right) = -31kJ/mol.$$

The work required to create a (111) surface of solid Cu_2O may be expressed as:

$$-N_O^{Cu_2O}[2.5\varepsilon_{OO} + 0.5\varepsilon_{Cu'O} + 6\varepsilon_{Cu'Cu'}],$$

where $N_O^{Cu_2O}$ is the number of oxygen moles per unit area at the Cu_2O (111) surface in each of the two oxygen planes associated with the outermost Cu plane. The surface unit cell of Cu_2O(111) shown in Fig. 2 contains one surface O-atom, and has an area of $a^2_{Cu_2O}\sqrt{3}$, where $a_{Cu_2O}=0.4267$ nm [32]. Thus the number of moles of oxygen per unit area is $1/(6.02\times10^{23}$ [atoms/mol] $a^2_{Cu_2O}\sqrt{3}$[m^2/atom]). No values of the surface energy of solid Cu_2O are available. However, the surface energy of the liquid is reported as 0.48 J/m^2 [33]. We estimate the surface energy of the solid to be 15% higher than that of the liquid (typical of the relative values in pure metals) and employ the method used above to evaluate ε_{CuCu} to obtain:

$$[2.5\varepsilon_{OO} + 0.5\varepsilon_{Cu'O} + 6\varepsilon_{Cu'Cu'}] = -104.5kJ/mol$$

As can be seen, there is not sufficient data to define all five of the bond energies in the present scheme, so that some additional conditions need to be imposed. Thus, we assume that the solution of Cu′ in Cu is ideal, i.e. that:

$$\varepsilon_{Cu'Cu} = 0.5(\varepsilon_{Cu'Cu'} + \varepsilon_{CuCu}).$$

We also assume that ε_{OO} is positive and that $\varepsilon_{Cu'O}$ is negative, both of which are plausible since there is likely to be some charge transfer between O and Cu, as has been suggested by first principles calculations [4]. Finally, we impose one further condition, namely that the solubility of O in liquid Cu in equilibrium with Cu_2O at 1365 K (just above the melting point of Cu) is close to the experimental value of 2at.% [34]. This limits the possible values of the bond energies to the free choice of one bond energy, as will be discussed after the scheme to calculate the O-solubility is described.

2.4. Calculation of the solubility of O in Cu

We determine the O-solubility in Cu by applying the common tangent construction to a free energy diagram of the bulk O-solution and of the coexisting Cu_2O phase. The free energy of the bulk O-solution can be extracted from the expression for the free energy per mole of solution given in Eq. (7). By substituting for $F^b(X_{Ob})$ from Eq. (6), we have:

$$F_m = \frac{1}{(2+X_{Ob})}\{4X_{Ob}[X_{Ob}\varepsilon_{OO} + \varepsilon_{Cu'O}] + 12\left[f^{(b)}_{CuCu}\varepsilon_{CuCu} + f^{(b)}_{Cu'Cu}\varepsilon_{Cu'Cu} + f^{(b)}_{Cu'Cu'}\varepsilon_{Cu'Cu'}\right] + RT[X_{Ob}\ln(X_{Ob}) + (1-X_{Ob})\ln(1-X_{Ob})]\} \quad (10)$$

In the limit $X_{Ob}\to1$ (or $X_O^C\to1/3$), i.e. when all O-sites are filled, the bulk solution becomes identical with the compound Cu_2O. Thus, over the range $0\le X_{Ob}\le1$ (or $0\le X_O^C\le\frac{1}{3}$), F_m represents the molar free energy of the Cu–O system ranging from pure Cu to $Cu_{0.67}O_{0.33}$, and can therefore be used to evaluate the solubility of the Cu–O-solution in equilibrium with Cu_2O by the common tangent construction.

The constraint of fixing the O-solubility at $X_O^C\approx0.02$ gives rise to a linear relationship between $\varepsilon_{Cu'Cu'}$ and ε_{OO}:

$$\varepsilon_{OO} = 83 + 3\varepsilon_{Cu'Cu'}(kJ/mol)$$

Values of $\varepsilon_{Cu'Cu'}$ more negative than about −23 kJ/mol lead to complete mutual solubility of Cu_2O and Cu, and are therefore incompatible with the desired solubility limit. Thus, the possible bond energies are completely defined by the choice of a single bond energy. From now on we will describe the bond energies used in any examples by specifying $\varepsilon_{Cu'Cu'}$.

2.5. Oxygen partial pressure

It is useful to compute the oxygen partial pressure, pO_2, in equilibrium with a given state of the Cu–O-solution, since most of the measurements on changes in the surface energy of Cu as a result of O-adsorption have been reported as a function of that variable.

The activity of O, a_O, in the solution is evaluated from the known O-chemical potential (Eq. (8)) as follows:

$$\mu_O-\mu_O^0 = RT\ln\left(a_O/a_O^0\right) \quad (11)$$

where μ_O^0 and a_O^0 are the O-chemical potential and O-activity in the standard state, respectively. For convenience, the standard state is defined as the O-solution in equilibrium with Cu_2O, i.e. μ_O^0 is just μ_O evaluated at $X_O^C=0.02$ for a temperature of 1365 K, and for which $a_O^0=1$ by definition. Since the O_2 is diatomic in the gas phase, but dissolves in Cu as an atomic species:

$$a_O = \left(pO_2/pO_2^0\right)^{1/2} \quad (12)$$

where pO_2^0 is the partial pressure of oxygen in the standard state, i.e. the partial pressure of oxygen in equilibrium with Cu_2O. Combining Eqs. (11) and (12):

$$pO_2 = pO_2^0 \exp\left[\frac{2\left(\mu_O - \mu_O^0\right)}{RT}\right] \tag{13}$$

At 1365 K (the temperature at which evaluations are performed) $pO_2^0 = 5\times10^{-6}$ atm [34].

3. Results and discussion

The equilibrium O-adsorption can be calculated by means of Eqs. (9a) and (9b). In Fig. 3 we show the effect on adsorption of changing the bond energies over the range -23 kJ/mol$<\varepsilon_{Cu'Cu'}<0$ kJ/mol at 1365 K. Four examples are given for the bond energy choices listed in Table 2. Fig. 3 are plots of the variation of the fractions of occupied O1 and O2-sites with increasing bulk oxygen concentration, extending all the way to the solubility limit. Fig. 3a and b display first order adsorption transitions, from a state of low adsorption to a state of high adsorption, as the bulk concentration of oxygen is increased. Such transitions have been predicted previously by segregation models in a number of different contexts [13,35–37] and have been observed experimentally in solid metallic alloys [38–40]. The transitions do not occur for the bond energy choices of Fig. 3c and d. In addition, as the bond energies change from Fig. 3a to d, (i.e. to less negative values of $\varepsilon_{Cu'Cu'}$) they produce a reversal in the relative adsorptions in the two O-layers associated with the $Cu^{(1)}$ plane. In Fig. 3a, adsorption is stronger in the O1-sites, whereas it is stronger in the O2-sites in Fig. 3b. It is worth noting that O1 and O2-sites have often been referred to in the literature as "on-top" and "sub-surface" sites, respectively. In Fig. 3c and d, the continuing change to less negative $\varepsilon_{Cu'Cu'}$ progressively decreases the adsorption in the O1-sites, until it essentially vanishes in Fig. 3d, whereas the O2-sites continue to reach O-saturation, as the limit of O-solubility is approached.

It is also useful to consider the corresponding changes in surface energy that result from O-adsorption. The surface energy can be

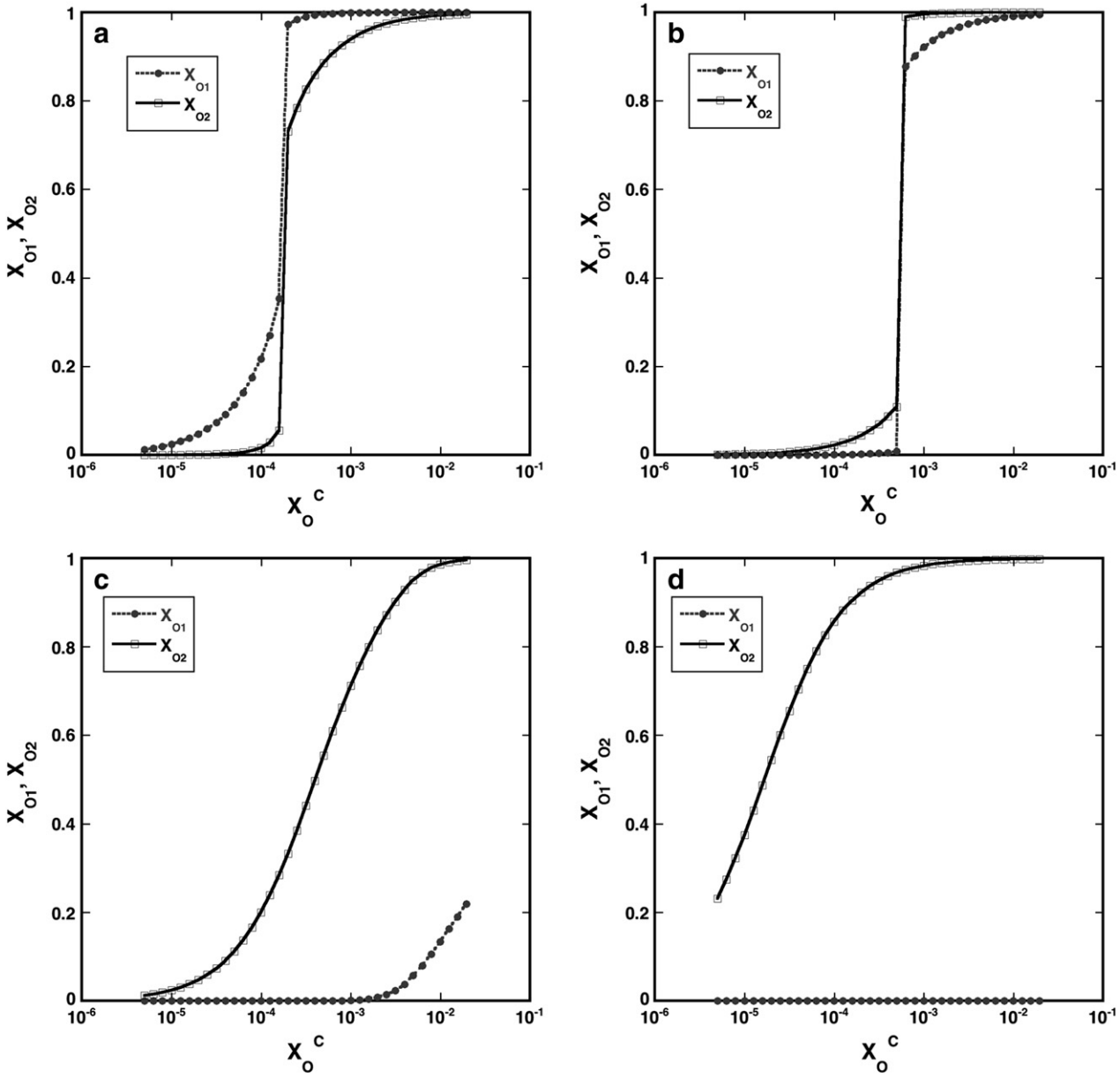

Fig. 3. Plots of near-surface O-site fractions vs. bulk composition for various values of $\varepsilon_{Cu'Cu'}$: (a) -23 kJ/mol, (b) -19 kJ/mol, (c) -13 kJ/mol, (d) -5 kJ/mol.

Table 2
Bond energies used in examples (kJ/mol).

$\varepsilon_{Cu'Cu'}$	$\varepsilon_{Cu'Cu}$	$\varepsilon_{Cu'O}$	ε_{OO}	ε_{CuCu}
−23	−27	−3	14	−31
−19	−25	−111	26	−31
−13	−22	−273	44	−31
−5	−18	−489	68	−31

computed by means of Eq. (3), together with the expressions for adsorption and chemical potential of Eqs. (4) and (8), and the equilibrium values of X_{O1} and X_{O2} from Eqs. (9a) and (9b). The results are displayed in Fig. 4, as a plot of surface energy versus oxygen partial pressure, the latter being calculated by means of Eq. (13). The sets of bond energies used for illustration in Fig. 4 are identified in the legend, and correspond to those used in Fig. 3. The curves of Fig. 4 are also labeled "a" through "d" for reference to Fig. 3a to d.

As expected from the Gibbs adsorption isotherm, the slopes of the variation in surface energy with $\log(pO_2)$ in Fig. 4 are proportional to the adsorption. In general, at low pO_2 (or correspondingly low X_O^C in Fig. 3) the adsorption is negligible, and the slopes of the curves in Fig. 4 are essentially zero. As pO_2 increases towards its maximum value at the limit of solubility, the slopes of the curves increase in absolute value. In cases such as those of Fig. 3a, b and d, where O-adsorption reaches a constant value at high X_O^C, the slopes of the corresponding curves in Fig. 4 also approach a constant value at higher pO_2, proportional to the maximum O-adsorption. Thus, the slopes of curves "a", and "b" in Fig. 4 reach a higher absolute value, corresponding to a maximum O-adsorption where both O1 and O2-sites are fully occupied, whereas curve "d" reaches a slope about half as steep because the O2-sites are filled but the O1-sites remain vacant. Curve "c" of Fig. 4 displays an intermediate slope, as the O1-sites in that case are only partly occupied at the O-solubility limit.

One other issue is worth noting, for example in the case of curve "a" of Fig. 4. The first order adsorption transition that occurs in that case (Fig. 3a) produces a sharp break in slope in curve "a" which separates the low adsorption from the high adsorption regime.

We now proceed to a comparison of the predictions of the model with experimental data on the changes in surface energy of liquid Cu associated with O-adsorption. All of the data obtained at temperatures between 1365 and 1375 K [20–23] are summarized in Fig. 5. The best fit to the data occurs for curve "d" of Fig. 4, corresponding to the fourth set of bond energies displayed in Table 2 ($\varepsilon_{Cu'Cu'} = -5$ kJ/mol). It should be mentioned here that the value of the surface energy of pure liquid Cu used in the determination of model bond energies was obtained by averaging all of the experimental measurements displayed in Fig. 5 over the range $10^{-22} < pO_2 < 10^{-14}$ atm. One important conclusion that emerges from the good fit with experiment of the slope predicted by the model at relatively high pO_2, is that the maximum experimental O-adsorption also corresponds to filling only half of the O-adsorption sites, specifically all of the O2 sites. By applying the Gibbs adsorption isotherm to the maximum (negative) slope predicted by the model in Fig. 5, it is possible to compute an O-adsorption of $\sim 7.1 \times 10^{-6}$ mol/m^2. This corresponds to about one adsorbed O-atom per four Cu surface atoms, consistent with filling all of the O2-adsorption sites. However, the experimental results do not provide any information on whether the upper or lower oxygen sites are occupied. Some insights into this issue may be gained by considering other modeling results.

As mentioned in the introduction, there has been significant activity using first principles methods that has focused on the interaction of oxygen with Cu surfaces. That work has addressed oxygen adsorption on various surface orientations of solid Cu, and may not reflect the behavior of oxygen at the surface of *liquid* Cu. Nevertheless, some of the issues studied may provide indications of trends, especially the work performed on the solid Cu(111) surface.

Calculations by Soon et al. [4] have investigated the relative stability of various O-adsorption sites on Cu(111). At low oxygen coverage, they find that the most stable site is the "on-top" site, which corresponds to our O1-site, whereas at higher coverage the on-top and sub-surface site (our O2-site) become comparable in stability. However, at solid Cu surfaces, there are elastic strain energy effects that are absent in adsorption at the liquid surface. For example, in discussing O-adsorption at Ag(111) surfaces, Li et al. [41] point out that the lower stability of sub-surface sites is due primarily to distortion of the Ag lattice. The results we have shown in Fig. 3 clearly indicate that the relative stability of O1 and O2-sites depends on the choice of bond energies, and that some sets of bond energies favor O1-sites, while others favor O2-sites, as can be seen for example by comparison of Fig. 3a and d.

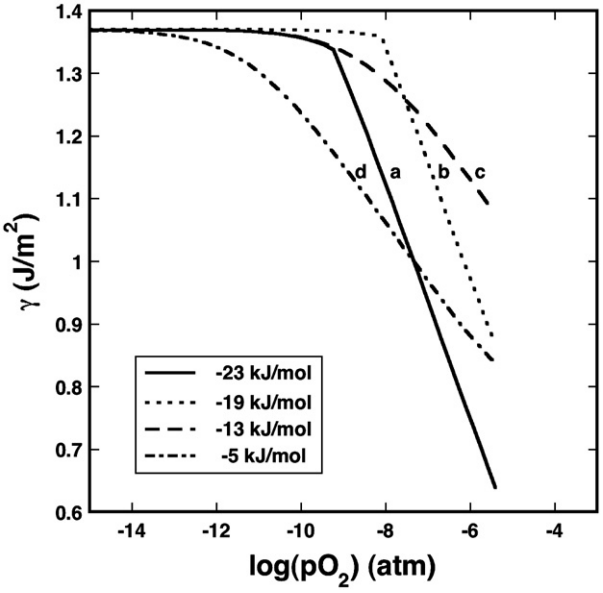

Fig. 4. Plots of calculated surface energy vs. oxygen partial pressure for various values of $\varepsilon_{Cu'Cu'}$, as indicated in the legend. Curves are also labeled "a" to "d" for reference to Fig. 3a to d.

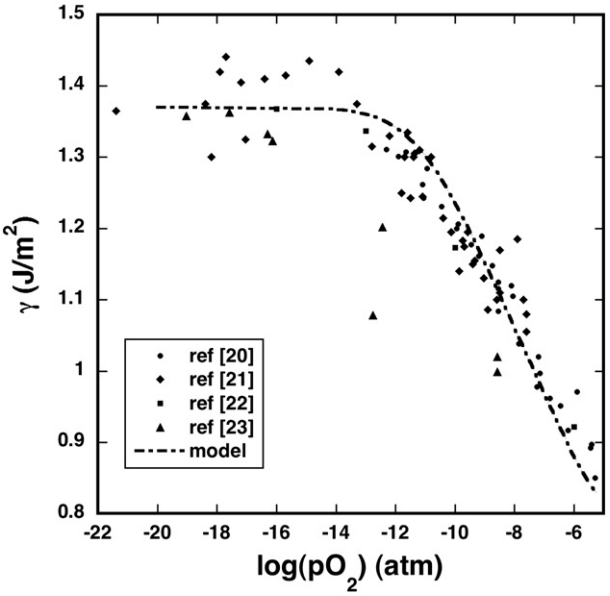

Fig. 5. Surface energy of liquid Cu as a function of O-partial pressure. Points represent measurements [20–23] and the line is the one labeled "d" in Fig. 4, corresponding to a bond energy choice of $\varepsilon_{Cu'Cu'} = -5$ kJ/mol in the model.

Another issue addressed by previous calculations is the possible formation of 2-d oxide layers for values of pO_2 below those where bulk Cu_2O is stable. For Cu(111), Soon et al. [4] have found that as the O-chemical potential is increased there is essentially no O-adsorption at the Cu surface prior to formation of a sequence of 2-d oxides (each having a somewhat different p4-type structure). This situation is not very different from that displayed in Fig. 3b, where the fraction of occupied O1 + O2-sites on the low side of the adsorption transition is only about 5%, and where the state of the system on the high side of the adsorption transition amounts essentially to a 2-d oxide of composition Cu_2O.

Finally, it should be noted that sufficient data to define all of the model parameters (bond energies) are unavailable, thereby leading to one adjustable parameter. As a result, the model cannot currently be used in a completely predictive manner. Nevertheless, by fitting the model to the measured pO_2 dependence surface energy of liquid Cu, one can conclude that O-adsorption to Cu surface is likely to be confined to O2-type, i.e. sub-surface, sites. Furthermore, the predictions of the model over the range of adjustable parameters seem to be consistent with several possible configurations of adsorbed oxygen that have been predicted by first principles calculations.

4. Conclusions

A model of O-adsorption to the liquid Cu surface has been constructed. This differs from previous models of O-adsorption, in that it specifies adsorption sites in a realistic manner. The model contains one adjustable parameter. As this parameter is varied, it produces a variety of possible adsorption characteristics, including the possibility of first order transitions which lead to the formation of 2-d surface oxide layers, and different sequences for the occupancy of adsorption sites.

Fitting the model to the experimental variation of the surface energy of liquid Cu with O-partial pressure fixes the adjustable parameter. The adsorption behavior that corresponds to this choice of parameters, indicates that O-adsorption to the surface of liquid Cu most likely occurs in sub-surface sites.

Acknowledgments

SC and DC wish to thank the European Community's Seventh Framework Program (FP7/2007-2013) for facilitating the work reported in this publication, under grant agreement n° FP7-NMP-2009-CSA-233484, and PW wishes to acknowledge with thanks the support of his research by the MRSEC Program of the National Science Foundation under Award No. DMR-0520425.

Appendix I

We provide here an explanation of the first term of Eq. (3):

$$3X_{O1}\varepsilon_{Cu'O} + 4X_{O2}\varepsilon_{Cu'O} + 3X_{O1}X_{O2}\varepsilon_{OO} + 0.5X_{O1}X_{Ob}\varepsilon_{OO} + 2X_{O2}X_{Ob}\varepsilon_{OO}$$

With the help of Figs. 1 and 2, it can be seen that 3 Cu′–O bonds are formed for each occupied O1-site, accounting for an energy of $3X_{O1}\varepsilon_{Cu'O}$; for each occupied O2-site 4 Cu′–O bonds are formed, which amount to an energy of $4X_{O2}\varepsilon_{Cu'O}$; each occupied O2-site also makes 3 bonds with the upper O-atoms, O1 (the energy is thus $3X_{O1}X_{O2}\varepsilon_{OO}$); each occupied O1-site is also connected to a lower O-site of $Cu^{(2)}$ with an occupancy probability of X_{Ob}, for an energy of $0.5X_{O1}X_{Ob}\varepsilon_{OO}$ (here the factor of 0.5 corrects for double counting when that bond is counted again from the second site); finally the term $2X_{O2}X_{Ob}\varepsilon_{OO}$ accounts for O–O interactions of an occupied O2-site with its 4 remaining O-neighbors (divided by two for double counting).

Appendix II

The chemical potential of component B in a binary A–B solution may be expressed in terms of the molar free energy of the solution (F_m) as:

$$\mu_B = F_m + (1-X_B)dF_m / dX_B$$

In the case of interest here, this may be rewritten as:

$$\mu_O = F_m + \left(1-X_O^C\right)dF_m / dX_O^C$$

To evaluate this expression, we transform the quantities defined in terms of X_O^C into ones defined as functions of X_{Ob}, using the relationships of Eqs. (5) and (7). Together with the chain rule, this yields:

$$\mu_O = \frac{F^b(X_{Ob})}{2N_O(2+X_{Ob})} + \frac{2}{(2+X_{Ob})}\frac{d}{dX_{Ob}}\left(\frac{F^b(X_{Ob})}{2N_O(2+X_{Ob})}\right)\frac{dX_{Ob}}{dX_O^C}$$

which simplifies to:

$$\begin{aligned}\mu_O &= \frac{1}{2N_O}\frac{dF^b(X_{Ob})}{dX_{Ob}} \\ &= [8X_{Ob}\varepsilon_{OO} + 4\varepsilon_{Cu'O}] + 12\left[\frac{\partial f^{(b)}_{CuCu}}{\partial X_{Ob}}\varepsilon_{CuCu} + \frac{\partial f^{(b)}_{Cu'Cu}}{\partial X_{Ob}}\varepsilon_{Cu'Cu} + \frac{\partial f^{(b)}_{Cu'Cu'}}{\partial X_{Ob}}\varepsilon_{Cu'Cu'}\right] \\ &\quad + RT[\ln(X_{Ob}/1-X_{Ob})]\end{aligned}$$

References

[1] F. Jensen, F. Besenbacher, E. Laegsgaard, I. Stensgaard, Surf. Sci. 259 (1991) L774.
[2] T. Matsumoto, R.A. Bennett, P. Stone, T. Yamada, K. Domen, M. Bowker, Surf. Sci. 471 (2001) 225.
[3] S.M. Johnston, A. Mulligan, V. Dhanak, M. Kadodwala, Surf. Sci. 519 (2002) 57.
[4] A. Soon, M. Todorova, B. Delley, C. Stampfl, Phys. Rev. B 73 (2006) 165424.
[5] P. Wynblatt, Annu. Rev. Mater. Res. 38 (2008) 173.
[6] E. Saiz, R.M. Cannon, A.P. Tomsia, Annu. Rev. Mater. Res. 38 (2008) 197.
[7] M.S. Daw, S.M. Foiles, M.I. Baskes, Mater. Sci. Rep. 9 (1993) 251.
[8] A. Landa, P. Wynblatt, A. Girshick, V. Vitek, A. Ruban, H. Skriver, Acta Mater. 46 (1998) 3027.
[9] B.C. Han, A. Van der Ven, G. Ceder, B.J. Hwang, Phys. Rev. B 72 (2005) 205409.
[10] D. McLean, Grain Boundaries in Metals, Oxford Press, London, 1957, p. 116.
[11] R. Defay, I. Prigogine, A. Bellmans, D.H. Everett, Surface Tension and Adsorption, Wiley, New York (NY), 1966, p. 158.
[12] P. Wynblatt, D. Chatain, Metal. Mater. Trans. A 37 (2006) 2595.
[13] P. Wynblatt, A. Saul, D. Chatain, Acta Mater. 46 (1998) 2337.
[14] P. Wynblatt, R.C. Ku, Surface segregation in alloys, in: W.C. Johnson, J.M. Blakely (Eds.), Interfacial Segregation, ASM, Metals Park (OH), 1979, p. 115.
[15] C. Antion, D. Chatain, Surf. Sci. 601 (2007) 2232.
[16] S. Iarlori, P. Carnevali, F. Ercolessi, E. Tosatti, Surf. Sci. 211 (1989) 55.
[17] F. Celestini, F. Ercolessi, E. Tosatti, Phys. Rev. Lett. 78 (1997) 3153.
[18] B.C. Lu, R.A. Rice, J. Chem. Phys. 68 (1978) 5558.
[19] O.M. Magnussen, M.J. Regan, E.H. Kawamoto, B.M. Ocko, P.S. Pershan, N. Maskil, M. Deutsch, S. Lee, K. Penanen, L.E. Berman, Phys. B 221 (1996) 257.
[20] B. Gallois, C.H.P. Lupis, Metal. Trans. B 12 (1981) 549.
[21] V. Ghetta, J. Fouletier, D. Chatain, Acta Mater. 44 (1996) 1927.
[22] S.P. Mehotra, A.C.D. Chaklader, Metall. Trans. B 16 (1985) 567.
[23] P.D. Ownby, J. Liu, J. Adhesion Sci. Technol. 2 (1988) 255.
[24] E. Ricci, A. Passerone, J.C. Joud, Surf. Sci. 206 (1988) 533.
[25] N. Eustathopoulos, B. Drevet, M.L. Muolo, Mater. Sci. Eng. A300 (2001) 34.
[26] C. Wagner, Acta Metal. 21 (1973) 1297.
[27] T. Chiang, Y.A. Chang, Metal. Trans. B 7 (1976) 453.
[28] Y.A. Chang, D.C. Hu, Metal. Trans. B 10 (1979) 43.
[29] M.L. Saboungi, P. Cerisier, M. Blander, Metal. Trans. B 13 (1982) 429.
[30] G. Belton, Metal. Trans. B 7 (1976) 35.
[31] T.E. Faber, Introduction to the Theory of Liquid Metals, University Press, Cambridge (UK, 1972.
[32] J.D.H. Donnay, Crystal Data Determinative Tables, 2nd editionAmerican Crystallographic Association, Washington (DC), 1963.
[33] S.Y. Sun, L. Zhang, S. Jahanshahi, Metal. Mater. Trans. B 34 (2003) 517.
[34] B. Hallstedt, D. Risold, L.J. Gaukler, J. Phase Equilibria 15 (1994) 483.
[35] C.R. Helms, Surf. Sci. 69 (1977) 689.
[36] P. Wynblatt, Y. Liu, J. Vac. Sci. Technol. A10 (1992) 2709.
[37] W.-C. Cheng, P. Wynblatt, Surf. Sci. 364 (1996) 409.
[38] J. Eugene, B. Aufray, F. Cabane, Surf. Sci. 241 (1991) 84.
[39] Y. Liu, P. Wynblatt, Surf. Sci. 290 (1993) 335.
[40] W.-C. Cheng, P. Wynblatt, Surf. Sci. 303 (1994) 179.
[41] W.X. Li, C. Stampfl, M. Scheffler, Phys. Rev. B 67 (2003) 045408.